IEEE Photonics Journal
An IEEE Photonics Society Publication

Open Access

A High-Performance and Temperature-Insensitive Shape Sensor Based on DPP-BOTDA

Volume 10, Number 01, February 2018

Dexin Ba
Chen Chen
Cheng Fu
Danyang Zhang
Zhiwei Lu
Zhigang Fan
Yongkang Dong

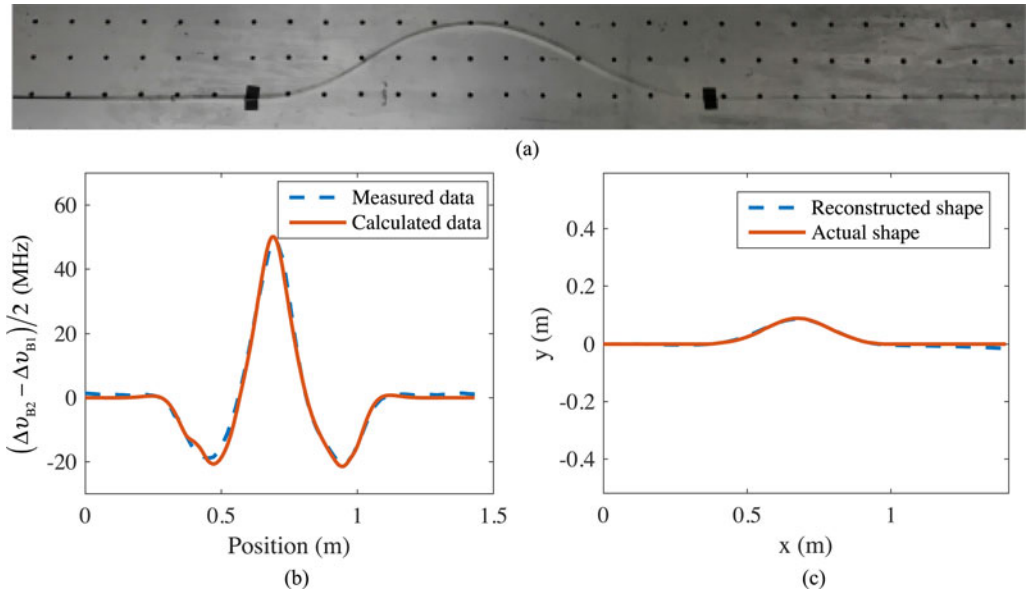

DOI: 10.1109/JPHOT.2017.2783956
1943-0655 © 2017 IEEE

IEEE photonics SOCIETY

IEEE

A High-Performance and Temperature-Insensitive Shape Sensor Based on DPP-BOTDA

Dexin Ba,[1] Chen Chen,[1] Cheng Fu,[1] Danyang Zhang,[1] Zhiwei Lu,[1] Zhigang Fan,[2] and Yongkang Dong[1]

[1]National Key Laboratory of Science and Technology on Tunable Laser, Harbin Institute of Technology, Harbin 150001, China
[2]Research Center for Space Optical Engineering, Harbin Institute of Technology, Harbin 150001, China

DOI:10.1109/JPHOT.2017.2783956
1943-0655 © 2017 IEEE. Translations and content mining are permitted for academic research only. Personal use is also permitted, but republication/redistribution requires IEEE permission. See http://www.ieee.org/publications_standards/publications/rights/index.html for more information.

Manuscript received August 24, 2017; revised November 29, 2017; accepted December 12, 2017. Date of publication December 18, 2017; date of current version January 11, 2018. This work was supported in part by the NSF of China under Grant 61605034, Grant 61308004, and Grant 61575052, in part by the China Postdoctoral Science Foundation under Grant 2016M591531, in part by the Postdoctoral Foundation of Heilongjiang Province under Grant LBH-Z15076, in part by the National Key Laboratory Funds for National Key Laboratory of Science and Technology on Tunable Laser, in part by the Fundamental Research Funds for the Central Universities under Grant NSRIF 2015041, in part by the National Key Scientific Instrument and Equipment Development Project of China under Grant 2013YQ040815 and Grant 2017YFF0108700. Corresponding author: Yongkang Dong (e-mail: aldendong@gmail.com).

Abstract: Distributed optical fiber strain sensing significantly increases the number of sensing points compared with fiber Bragg grating sensor, which makes it an excellent candidate for shape sensing. Theoretical analysis indicates that the spatial resolution of strain measurement is crucial to the performance of shape sensing, so a shape sensor based on differential pulse-width-pair Brillouin optical time-domain analysis is proposed to improve the spatial resolution and shape sensing performance. The sensing fiber is attached on the both sides of a steel strip substrate, which enables the measurement of Brillouin frequency shifts (BFSs) of both the sides to suppress temperature crosstalk. In the experiment, first, the dependence of BFS variation on the curvature of the fiber is measured, the result of which agrees well with theory. Then the reconstruction of three shapes are demonstrated, the spatial resolution of which is 10 cm.

Index Terms: Fiber-optic shape sensor, Brillouin optical time-domain analysis, differential pulse-width pair, temperature-insensitive.

1. Introduction

In recent decades, fiber-optic shape sensing technology has received great attention for its wide range of potential application areas such as medicine, architecture, aeronautics and intelligent structural systems, where it plays an important role in tracking the path of flexible instruments [1]–[4]. A great deal of researches have been devoted to the development of shape sensors based on fiber Bragg grating (FBG) [5]–[9]. Generally, these shape sensors require FBG array or network. Once the complexity of the shape to be measured increases, the interval between FBGs should be shortened, which results in the increasing of the number of FBGs. All of them lead to the difficulties in manufacturing and signal demodulation. In contrast to these point sensors, distributed

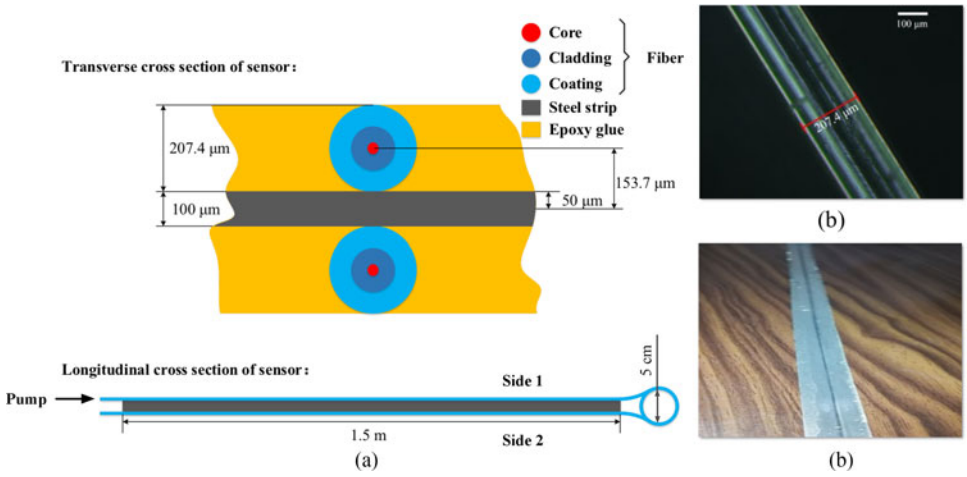

Fig. 1. (a) Sketch map of the shape sensor; (b) Micrograph of the PMF; (c) Photograph of the shape sensor.

Brillouin optical fiber sensor can measure arbitrary position along the fiber [10]–[15], which makes it an excellent candidate for shape sensing, especially for complex shapes and flexible objects. Wylie *et al.* have demonstrated a shape sensor based on Brillouin optical time-domain analysis (BOTDA) enhanced by dark pulse, the spatial resolution of which is 25 cm [16]. Using multi-core fiber, Thévenaz *et al.* realized two-dimensional shape sensing, the spatial resolution of which is 20 cm [17].

Shape sensing based on distributed Brillouin sensing is realized by the measurement of strain. The precision of strain measurement is mainly degraded by the limited spatial resolution and temperature drift which derives from heat dissipation of motors. In this paper, the influence of spatial resolution on the shape reconstruction error is quantitatively studied, which indicates that the spatial resolution is crucial to the performance of shape sensing. In order to realize high-performance shape sensing, a shape sensor based on differential pulse-width-pair (DPP) BOTDA is proposed here, the spatial resolution of which is 10 cm. The sensing fiber is attached on both sides of the shape sensor, which enables the measurement of Brillouin frequency shifts (BFSs) of both the sides to suppress the temperature sensitivity. Four experiments are carried out to study its performance. Firstly, the curvature coefficient of the sensor is measured. Then two shape sensing experiments are carried out. At last, the temperature insensitivity of the shape sensor is demonstrated.

2. Sensor Design and Shape Reconstruction Algorithm

The sketch map of the shape sensor is shown in Fig. 1(a). A segment of polarization maintaining fiber (PMF) is glued on a 1.5-m stainless steel strip substrate by epoxy glue, which has been experimentally proved to have the ability of being bent easily after drying and solidifying. The PMF is glued on both sides of the strip, named as Side 1 and Side 2, to suppress the influence of temperature variation. The fiber length in the returning region is 50 cm, and the diameter of the circle in this region is 5 cm. Fig. 1(b) is the micrograph of PMF, and Fig. 1(c) is the photograph of the shape sensor.

The theoretical model of the shape sensor is simplified and shown in Fig. 2. R is the bending radius, and L is the initial length of the sensing section. d is the distance between the core of the fiber and the neutral axis of the steel strip. $\Delta\varepsilon_1$ and $\Delta\varepsilon_2$ are the strains of Side 1 and Side 2, which satisfy

$$\Delta\varepsilon_1 = \frac{d}{R} = -\Delta\varepsilon_2 \tag{1}$$

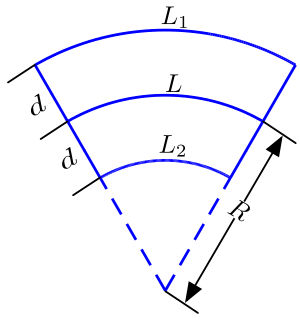

Fig. 2. Diagram of bending.

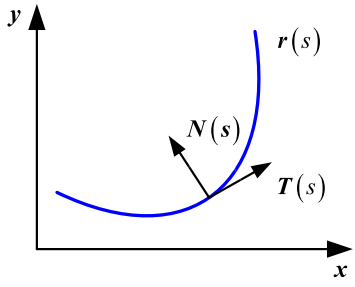

Fig. 3. Unit tangent vector $\boldsymbol{T}(s)$ and unit normal vector $\boldsymbol{N}(s)$.

The variation of BFS is determined by both temperature and strain [18]:

$$\Delta\upsilon_{\mathrm{B}} = C_{\mathrm{T}}\Delta T + C_{\varepsilon}\Delta\varepsilon \tag{2}$$

where C_{T} and C_{ε} are temperature and strain coefficients related to BFS, respectively; ΔT is the variation of temperature. Because temperature is the same for both sides of the sensor, its effect on the variation of BFS can be suppressed by subtracting the BFSs of the double sides of the sensor. From (2), we have

$$\Delta\upsilon_{\mathrm{B2}} - \Delta\upsilon_{\mathrm{B1}} = -C_{\varepsilon}\frac{2d}{R} \tag{3}$$

Defining the curvature coefficient of BFS as:

$$C_{\kappa} = C_{\varepsilon}d \tag{4}$$

Equation (3) is rewritten as:

$$\Delta\upsilon_{\mathrm{B2}} - \Delta\upsilon_{\mathrm{B1}} = -2C_{\kappa}\frac{1}{R} = -2C_{\kappa}\kappa \tag{5}$$

where $\kappa = 1/R$ is the bending curvature.

A 2-D shape can be described as a vector $\boldsymbol{r}(s)$, where s is the arc length of the curve, as shown in Fig. 3. $\boldsymbol{r}(s)$ is the integral of unit tangent vector $\boldsymbol{T}(s)$, i.e.,:

$$\boldsymbol{r}(s) = \int \boldsymbol{T}(s)\,\mathrm{d}s + \boldsymbol{r}(0) \tag{6}$$

$\boldsymbol{T}(s)$ can be calculated accroding to the 2-D Frenet-Serret formulas [19]:

$$\begin{aligned}\frac{\mathrm{d}\boldsymbol{T}(s)}{\mathrm{d}s} &= \kappa(s)\,\boldsymbol{N}(s)\\ \frac{\mathrm{d}\boldsymbol{N}(s)}{\mathrm{d}s} &= -\kappa(s)\,\boldsymbol{T}(s)\end{aligned} \tag{7}$$

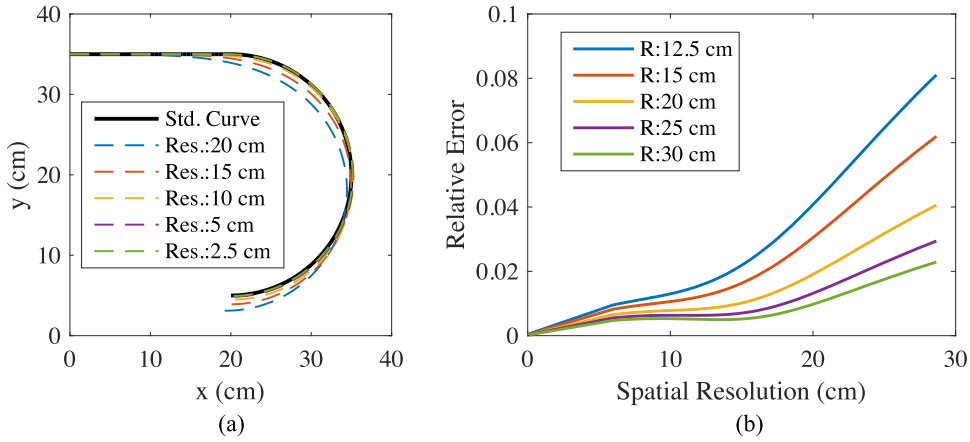

Fig. 4. (a) Simulated shape reconstruction with various spatial resolutions, ranging from 2.5 cm to 20 cm; (b) Relative error as a function of spatial resolution for semicircles with different radii, ranging from 12.5 cm to 30 cm.

where $\boldsymbol{N}(s)$ is the unit normal vector, and $\kappa(s)$ is the curvature. So the shape reconstruction can be carried out with three steps. Firstly, measure BFS along the fiber and calculate curvature $\kappa(s)$. Second, calculate $\boldsymbol{T}(s)$ with (7). At last, reconstruct shape with (6).

Spatial resolution is a key parameter of distributed Brillouin strain sensor. Using the model mentioned above, an analysis of its influence on the performance of shape reconstruction is carried out, the result of which is shown in Fig. 4(a). The black curve represents the shape to be retrieved, which consists of a semicircle (radius: 15 cm) connected with a 20-cm straight line. In the simulation, the shape is reconstructed with various spatial resolutions, ranging from 2.5 cm to 20 cm. As predicted, higher spatial resolution leads to more accurate shape sensing. According to the principle of the algorithm, the position of each point on the reconstructed shape is determined by the position and the tangential vector of previous point, so the position error accumulates gradually. Based on this reason, a relative error is defined to evaluate the performance of the shape reconstruction as follows:

$$E_r = \frac{\sqrt{(x_R - x_A)^2 + (y_R - y_A)^2}}{L} \tag{8}$$

where (x_A, y_A) and (x_R, y_R) are the actual and the reconstructed coordinates of the last point in the sensor, respectively. The relaiton between spatial resolution and relative error is shown in Fig. 4(b). The radius of the semicircle ranges from 12.5 cm to 30 cm (The curvature ranges from 3.3 m^{-1} to 8 m^{-1}). In this figure, there is a quasi-flat area starting from ~6 cm (x axis), where the relative error is less sensitive to the variation of spatial resolution. The width of the quasi-flat area decreases with the radius of the semicircle. For the 12.5-cm radius, the quasi-flat area ends at ~11.7 cm, where the relative error is 1.5%. It is economical to choose a corresponding spatial resolution in this range if permitted.

3. Experimental Setup

The experimental setup is shown in Fig. 5. A 1550-nm optical fiber laser with 40-kHz linewidth is used as light source, the output of which is divided into two branches by an optical coupler. In the upper branch, an electric-optic modulator (EOM1) is employed to modulate the continuous wave to pulses, which are then amplified by an erbium-doped fiber amplifier (EDFA) to a peak power of 0.5 W. As pump wave, the amplified pulses propagate into the sensing fiber, as shown in Fig. 1(a). In the lower branch, the light is modulated into double sidebands by EOM2, which is driven by a microwave generator (MG). The probe trace is detected by a photo detector (PD), the output of

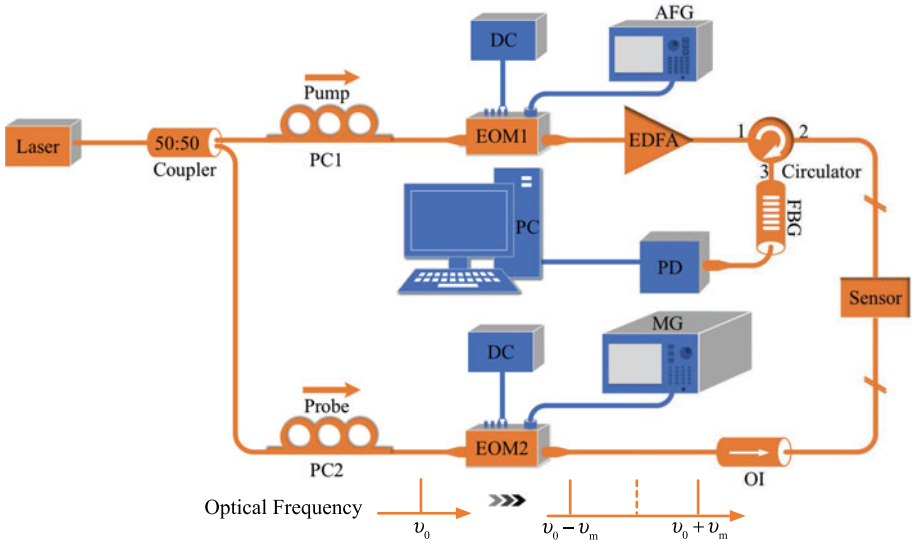

Fig. 5. Experimental setup. PC: polarization controller, EOM: electro-optic modulator, DC: direct current, AFG: arbitrary function generator, MG: microwave generator, EDFA: erbium-doped fiber amplifier, FBG: fiber Bragg grating, PD: photo detector, OI: optical isolator.

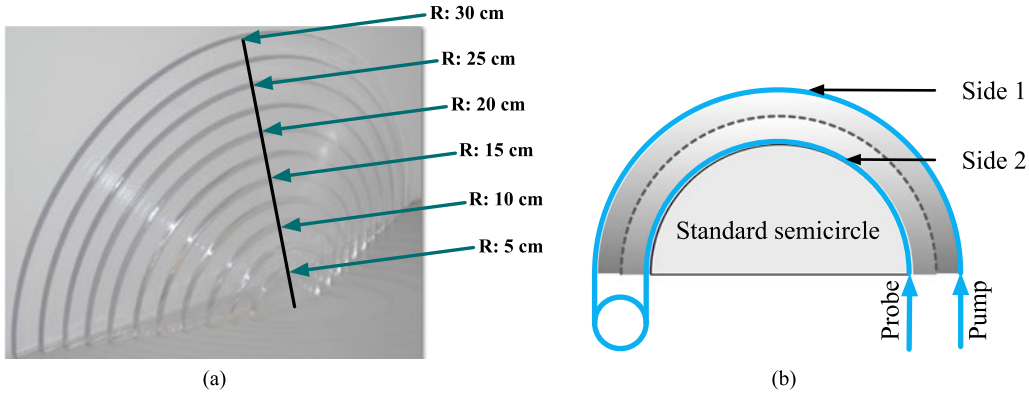

Fig. 6. (a) Standard semicircles; (b) Sketch map of shape sensing of the semicircles.

which is acquired by a DAQ (data acquisition) card. Before the PD, a fiber Bragg grating (FBG) is used to filter out the upper sideband.

According to our simulation, spatial resolution of strain measurement is a key parameter to determine the performance of the shape sensor. For a conventional BOTDA scheme, the minimum spatial resolution is limited to ~1 m [18], [20], [21]. Some techniques have been proposed to improve the spatial resolution to cm-scale [22]–[26]. In this experiment, a DPP-BOTDA is utilized, where an 8.5/8 ns pulse-pair is generated by the AFG to modulate the pump wave. The real spatial resolution is measured to be ~10 cm due to the signal broadening resulting from the bandwidth limitation of the DAQ card.

4. Results and Discussion

4.1 The Curvature Coefficient of Brillouin Frequency Shift

In order to measure the curvature coefficient of BFS and verify (5), an acrylic plate is cut into a series of standard semicircles (radius: 5 ~ 30 cm, step: 2.5 cm), as shown in Fig. 6(a). The shape sensor is attached on these standard semicircles, the sketch map of which is shown in Fig. 6(b).

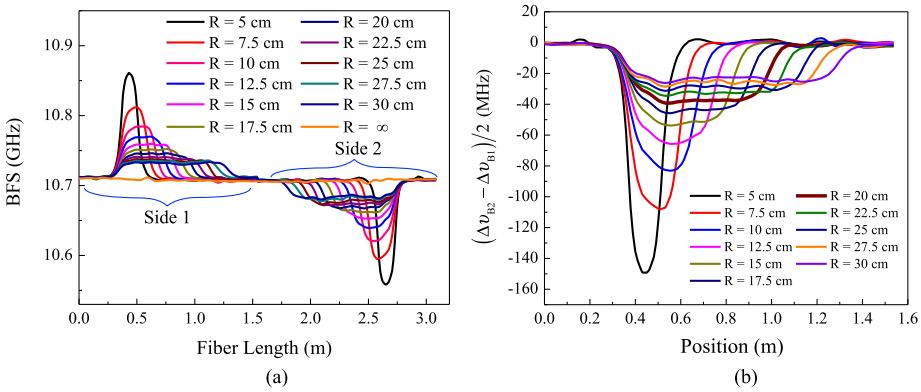

Fig. 7. (a) The measured BFS when sending of different semicircles; (b) The difference of BFS variation between Side 2 and Side 1.

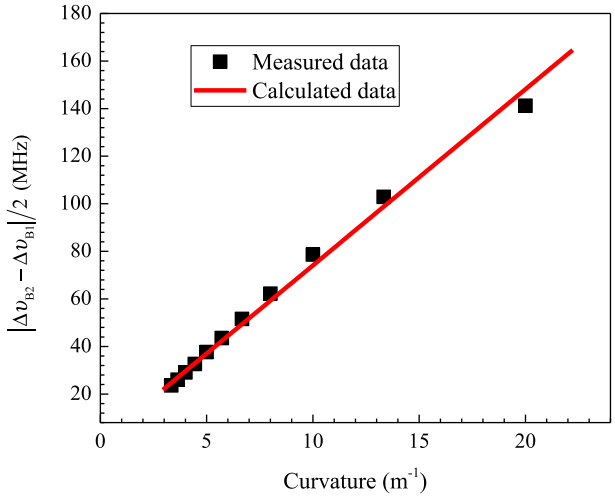

Fig. 8. Curvature dependence of the difference of BFS variation between the two sides of sensor.

The fiber on Side 1 of the shape sensor is stretched when being bent, while the fiber on the other side is compressed. The BFS along the fiber is measured for 3 times to improve the accuracy. As a reference, the BFS of the shape sensor without bending is also measured. The measured BFS along the fiber is shown in Fig. 7(a). The first 1.5-m fiber is on Side 1, where the BFS variation of bent part is greater than zero as predicted. The difference of BFS variation between Side 2 and Side 1 is calculated, the result of which is shown in Fig. 7(b).

Fig. 8 shows the curvature dependence of the difference of BFS variation between Side 1 and Side 2 of sensor. The black points represent the measured data, while the red curve is the calculated result using (5) with the Brillouin strain coefficient of 0.0482 MHz/$\mu\varepsilon$ [27]. The measured data is consistent with the theoretical result. The curvature coefficient C_κ is determined to be 7.4062 MHz $\cdot$ m via curve fitting. The corresponding Brillouin strain coefficient is 7.4062 MHz $\cdot$ m/153.7 μm $=$ 0.0482 MHz/$\mu\varepsilon$, which equals to the value in [20]. The error increases with the increase of curvature, especially in $\kappa = 20$ m^{-1} (R $=$ 5 cm), which derives from the limitation of spatial resolution.

4.2 Shape Sensing Experiments

Two shape sensing experiments are carried out in this section. In the first experiment, a shape as shown in Fig. 9(a) is reconstructed. The BFS along FUT is measured for 3 times for average, the

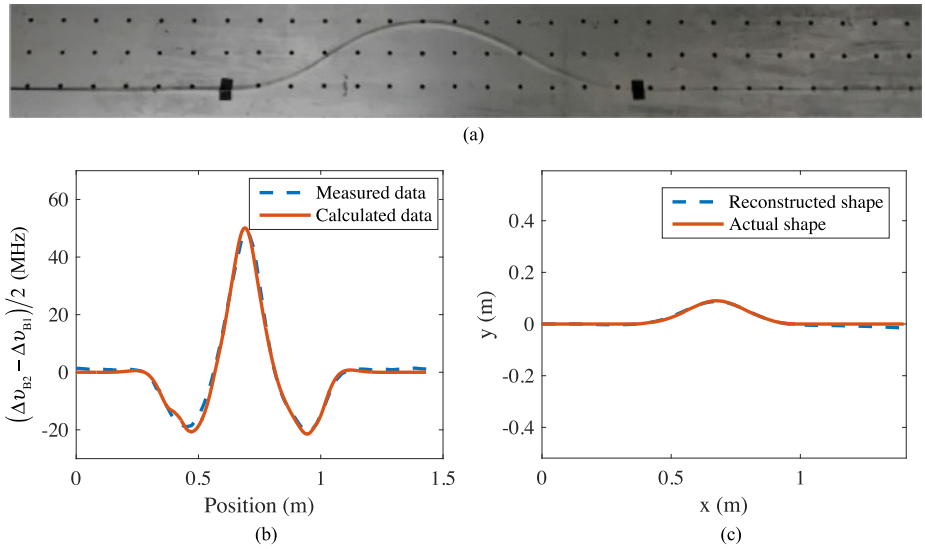

Fig. 9. (a) Photograph of the shape to be measured; (b) The measured and the theoretical BFS difference between Side 1 and Side 2 of the sensor; (c) The reconstructed shape.

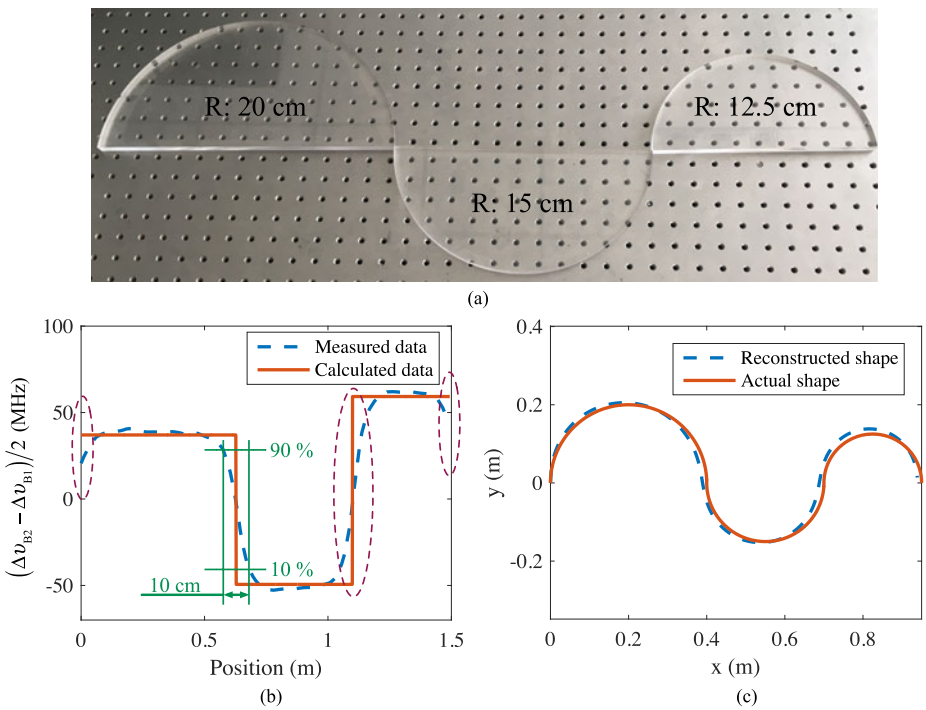

Fig. 10. (a) Photograph of the shape to be measured; (b) The measured and the theoretical BFS difference between Side 1 and Side 2 of the sensor. There are four step changes theoretically; (c) The reconstructed shape.

result of which is shown in Fig. 9(b). With the reconstruction algorithm stated in Section 2, the shape is reconstructed, which is plotted together with the actual shape in Fig. 9(c). The reconstructed shape accords with the actual curve. According to (8), its relative error is 1%.

Next, a reconstruction experiment of a shape with step-changed BFS is carried out. The shape to be retrieved is shown in Fig. 10(a). It consists of three semicircles, the radii of which are 20 cm, 15 cm and 12.5 cm, respectively. The measured BFS is drawn in Fig. 10(b) together with its theoretical

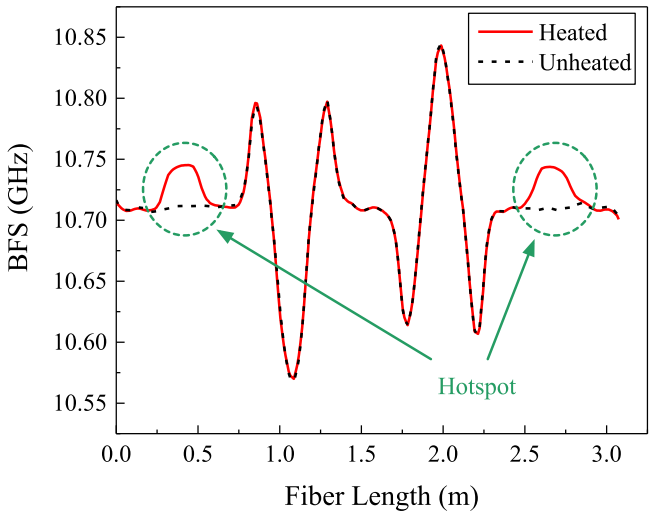

Fig. 11. Measured BFS with and without heating.

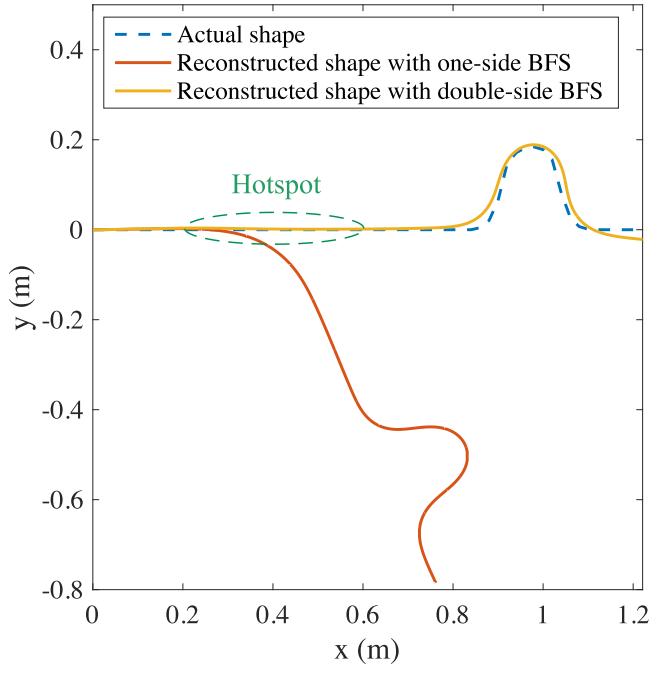

Fig. 12. Shape reconstructions with one-side and both-side BFS, respectively.

value. There are four step changes of BFS theoretically. The spatial resolution is estimated as the position difference from 10% to 90% of amplitude, which is 10 cm. The reconstructed shape is shown in Fig. 10(c). Because of the limitation of spatial resolution, the measured BFS deviates from its real value, which ultimately leads to the error of shape reconstruction. The relative error for the entire curve is 5%.

4.3 Temperature Insensitivity of the Shape Sensor

In order to verify the temperature insensitivity of the shape sensor, one part of the sensor is heated. The measured BFS is shown in Fig. 11 with red curve. The BFS before heating is measured for

reference, which is drawn in black dots. The hotspot locates from 0.25 m to 0.55 m, where the temperature increases by ∼30 °C. The reconstruction of the shape is shown in Fig. 12, where the red curve represents the reconstructed shape with only one side of the BFS data. The calculated shape starts to drift off at the hotspot. However, with the proposed method in Section 2, where double-side BFS is used, the effect of temperature variation is compensated successfully, which is shown with yellow curve in this figure.

5. Conclusion

In summary, a two-dimensional optical fiber sensor based on DPP-BOTDA (10-cm spatial resolution) is proposed and demonstrated, which is insensitive to temperature variation. Two shapes are reconstructed by the sensor, the total reconstruction errors of which are 1% and 5%, respectively. With a locally heated FUT, its temperature insensitivity is verified.

Both simulation and experiments prove that spatial resolution of strain measurement is crucial to shape sensing. According to our research of the relation between reconstruction error and spatial resolution, there is a quasi-flat area in the relation curve, where the relative error is less sensitive to the variation of spatial resolution. For one semicircular curve with the radius ranging from 12.5 cm to 30 cm, it is economical to choose the spatial resolution in the range from 6.0 cm to 11.7 cm, where the relative error is less than 1.5%. For a more precise sensing or for shape with larger curvature, a higher spatial resolution is required. Up to now, the best spatial resolution of DPP-BOTDA is 2 cm [28], which suggests that the performance of the shape sensor can be further improved by using a faster DAQ and AFG. Because the protocol of the shape sensor is based on BOTDA, techniques to improve the performance of BOTDA can be utilized in the shape sensor. Especially, to meet the demand of fast and real time monitoring, dynamic sensing techniques can be incorporated into the shape sensor [14], [29]–[31].

References

[1] M. S. van der Heiden *et al.*, "Accurate and efficient fiber optical shape sensor for MRI compatible minimally invasive instruments," *SPIE Opt. Syst. Des.*, vol. 8550, 2012, Art. no. 85500L.

[2] T. Paetz *et al.*, "Integration of fiber optical shape sensing with medical visualization for minimal-invasive interventions," *SPIE Med. Imaging*, vol. 9415, 2015, Art. no. 94150Z.

[3] K. Mandal, F. Parent, S. Martel, R. Kashyap, and S. Kadoury, "Vessel-based registration of an optical shape sensing catheter for MR navigation," *Int. J. Comput. Assisted Radiol. Surg.*, vol. 11, no. 6, pp. 1025–1034, 2016.

[4] E. M. Lally, M. Reaves, E. Horrell, S. Klute, and M. E. Froggatt, "Fiber optic shape sensing for monitoring of flexible structures," *SPIE Smart Struct. Mater. + Nondestructive Eval. Health Monitoring*, vol. 8345, 2012, Art. no. 83452Y.

[5] M. A. Davis, A. D. Kersey, J. Sirkis, and E. J. Friebele, "Shape and vibration mode sensing using a fiber optic Bragg grating array," *Smart Mater. Struct.*, vol. 5, no. 6, pp. 759–765, 1996.

[6] L. Zhang, J. Qian, L. Shen, and Y. Zhang, "FBG sensor devices for spatial shape detection of intelligent colonoscope," in *Proc. IEEE Int. Conf. Robot. Autom.*, vol. 1, pp. 834–840, 2004.

[7] H. Kim, L. Kang, and J. Han, "Shape estimation with distributed fiber Bragg grating sensors for rotating structures," *Smart Mater. Struct.*, vol. 20, no. 3, 2011, Art. no. 035011.

[8] J. Yi, X. Zhu, H. Zhang, L. Shen, and X. Qiao, "Spatial shape reconstruction using orthogonal fiber Bragg grating sensor array," *Mechatronics*, vol. 22, no. 6, pp. 679–687, 2012.

[9] K. R. Henken, J. Dankelman, J. J. Dobbelsteen, L. K. Cheng, and M. S. Heiden, "Error analysis of FBG-Based shape sensors for medical needle tracking," *IEEE/ASME Trans. Mechatronics*, vol. 19, no. 5, pp. 1523–1531, Oct. 2014.

[10] Y. H. Kim, K. Lee, and K. Y. Song, "Brillouin optical correlation domain analysis with more than 1 million effective sensing points based on differential measurement," *Opt. Exp.*, vol. 23, no. 26, pp. 33241–33248, 2015.

[11] M. A. Soto, M. Taki, G. Bolognini, and F. Di Pasquale, "Optimization of a DPP-BOTDA sensor with 25 cm spatial resolution over 60 km standard single-mode fiber using Simplex codes and optical pre-amplification," *Opt. Exp.*, vol. 20, no. 7, pp. 6860–6869, 2012.

[12] O. Shlomi, E. Preter, D. Ba, Y. London, Y. Antman, and A. Zadok, "Double-pulse pair Brillouin optical correlation-domain analysis," *Opt. Exp.*, vol. 24, no. 23, pp. 26867–26876, 2016.

[13] Y. Mizuno, Z. He, and K. Hotate, "Measurement range enlargement in Brillouin optical correlation-domain reflectometry based on temporal gating scheme," *Opt. Exp.*, vol. 17, no. 11, pp. 9040–9046, 2009.

[14] Y. Mizuno, N. Hayashi, H. Fukuda, K. Y. Song, and K. Nakamura, "Ultrahigh-speed distributed Brillouin reflectometry," *Light Sci. Appl.*, vol. 5, no. 12, 2016, Art. no. e16184.

[15] A. Denisov, M. A. Soto, and L. Thévenaz, "Going beyond 1000000 resolved points in a Brillouin distributed fiber sensor: Theoretical analysis and experimental demonstration," *Light Sci. Appl.*, vol. 5, no. 5, 2016, Art. no. e16074.

[16] M. T. V. Wylie, B. G. Colpitts, and A. W. Brown, "Fiber optic distributed differential displacement sensor," *J. Lightw. Technol.*, vol. 29, no. 18, pp. 2847–2852, Sep. 2011.
[17] Z. Zhao, M. A. Soto, M. Tang, and L. Thévenaz, "Distributed shape sensing using Brillouin scattering in multi-core fibers," *Opt. Exp.*, vol. 24, no. 22, pp. 25211–25223, 2016.
[18] X. Bao and L. Chen, "Recent progress in distributed fiber optic sensors," *Sensors*, vol. 12, no. 7, pp. 8601–8639, 2012.
[19] J. P. Moore and M. D. Rogge, "Shape sensing using multi-core fiber optic cable and parametric curve solutions," *Opt. Exp.*, vol. 20, no. 3, pp. 2967–2973, 2012.
[20] A. Motil, A. Bergman, and M. Tur, "[INVITED] State of the art of Brillouin fiber-optic distributed sensing," *Opt. Laser Technol.*, vol. 78, pp. 81–103, 2016.
[21] A. Fellay, L. Thévenaz, M. Facchini, M. Niklès, and P. Robert, "Distributed sensing using stimulated Brillouin scattering: Towards ultimate resolution," *presented at the 12th Int. Conf. Optical Fiber Sensors*, Williamsburg, VA, USA, 1997.
[22] K. Kishida and C.-H. Li, "Pulse pre-pump-BOTDA technology for new generation of distributed strain measuring system," in *Proc. Struct. Health Monitoring Intell. Infrastruct.*, 2005, pp. 471–477.
[23] S. M. Foaleng, M. Tur, J.-C. Beugnot, and L. Thévenaz, "High spatial and spectral resolution long-range sensing using Brillouin echoes," *J. Lightw. Technol.*, vol. 28, no. 20, pp. 2993–3003, Oct. 2010.
[24] T. Sperber, A. Eyal, M. Tur, and L. Thévenaz, "High spatial resolution distributed sensing in optical fibers by Brillouin gain-profile tracing," *Opt. Exp.*, vol. 18, no. 8, pp. 8671–8679, 2010.
[25] W. Li, X. Bao, Y. Li, and L. Chen, "Differential pulse-width pair BOTDA for high spatial resolution sensing," *Opt. Exp.*, vol. 16, no. 26, pp. 21616–21625, 2008.
[26] A. W. Brown, B. G. Colpitts, and K. Brown, "Dark-Pulse Brillouin optical time-domain sensor with 20-mm spatial resolution," *J. Lightw. Technol.*, vol. 25, no. 1, pp. 381–386, Jan. 2007.
[27] Y. Dong, L. Chen, and X. Bao, "High-spatial-resolution time-domain simultaneous strain and temperature sensor using Brillouin scattering and birefringence in a polarization-maintaining fiber," *IEEE Photon. Technol. Lett.*, vol. 22, no. 18, pp. 1364–1366, Sep. 2010.
[28] Y. Dong, H. Zhang, L. Chen, and X. Bao, "2 cm spatial-resolution and 2 km range Brillouin optical fiber sensor using a transient differential pulse pair," *Appl. Opt.*, vol. 51, no. 9, pp. 1229–1235, 2012.
[29] Y. Peled, A. Motil, and M. Tur, "Fast Brillouin optical time domain analysis for dynamic sensing," *Opt. Exp.*, vol. 20, no. 8, pp. 8584–8591, 2012.
[30] D. Ba *et al.*, "Distributed measurement of dynamic strain based on multi-slope assisted fast BOTDA," *Opt. Exp.*, vol. 24, no. 9, pp. 9781–9793, 2016.
[31] Y. Dong *et al.*, "High-spatial-resolution fast BOTDA for dynamic strain measurement based on differential double-pulse and second-order sideband of modulation," *IEEE Photon. J.*, vol. 5, no. 3, Jun. 2013, Art. no. 2600407.